

RESEARCH

Open Access



Identification and exploration of key genes associated with radioresistance in lung adenocarcinoma

Ying Wang^{1†}, Yangyang Shang^{2,3†}, Mingyu Hua¹, Yidi Wang⁴, Beina Hui¹, Weibin Hu¹, Mengke Zhu⁵, Xiaozhi Zhang^{1*} and Jing Li^{1*}

Abstract

Background Radiation resistance in lung adenocarcinoma (LUAD) remains a primary obstacle limiting radiotherapy efficacy. However, the detailed factors and molecular mechanisms influencing LUAD radiosensitivity are not fully understood.

Methods Radioresistance-related genes (RRRGs) were screened by RNA sequencing and bioinformatics analysis, and a prediction model for radiotherapy efficacy was developed via LASSO-Cox regression analysis. We specifically focused on Stanniocalcin 2 (STC2) due to its prognostic significance and validated its expression through immunohistochemical staining (IHC) in pathological samples from LUAD patients. A STC2 knockdown (siSTC2) A549 cell line was created, and Western blotting, CCK8, and colony formation assays were performed to investigate STC2's involvement in radioresistance.

Results An efficacy prediction model was constructed using 6 RRRGs (FCGBP, SLCO4A1, ALDH3A1, STC2, TERT, CYP24A1). IHC analysis of 74 LUAD patients showed significantly higher STC2 expression in radiotherapy non-responders (N-Res) versus responders (Res) ($p < 0.05$). Patients with elevated STC2 levels experienced shorter overall survival (OS). Western blotting revealed higher STC2 expression in irradiated (IR) A549 cells compared to non-irradiated (N-IR) ($p < 0.05$). CCK8 assays results suggested that knockdown of STC2 resulted in a significant reduction in cell proliferation ability ($p < 0.05$), and colony formation assays confirmed a significant decrease in clonogenic ability of siSTC2 cells compared to controls ($p < 0.05$).

Conclusion STC2 plays a significant role in mediating LUAD cell radioresistance, with high expression correlating with poor prognosis. Therefore, STC2 represents a promising therapeutic target for overcoming LUAD radioresistance.

Clinical trial number Not applicable.

Keywords Lung adenocarcinoma, Radiotherapy, Prognostic model, STC2, Radioresistance

[†]Ying Wang and Yangyang Shang contributed equally to this work.

*Correspondence:

Xiaozhi Zhang

zhangxiaozhi@xjtu.edu.cn

Jing Li

lijingkk21@163.com

¹Department of Radiation Oncology, The First Affiliated Hospital of Xi'an Jiaotong University, Xi'an, Shaanxi, China

²Center for Translational Medicine, The First Affiliated Hospital of Xi'an Jiaotong University, Xi'an, Shaanxi, China

³Key Laboratory for Tumor Precision Medicine of Shaanxi Province, The First Affiliated Hospital of Xi'an Jiaotong University, Xi'an, Shaanxi, China

⁴Department of Breast Surgery, The First Affiliated Hospital of Xi'an Jiaotong University, Xi'an, Shaanxi, China

⁵Department of Pathology, The First Affiliated Hospital of Xi'an Jiaotong University, Xi'an, Shaanxi, China



Introduction

Lung cancer remains a leading cause of cancer-related mortality worldwide [1, 2], with LUAD accounting for approximately 45% of all lung cancer cases [3]. Despite significant advances in treatment, the 5-year survival rate remains unsatisfactory, emphasizing the need for improved therapeutic approaches [1]. Radiotherapy is a fundamental treatment for advanced LUAD, yet its effectiveness is frequently hindered by radioresistance. This resistance involves complex interactions among DNA repair mechanisms, apoptosis regulation, and the tumor microenvironment [4]. Although substantial progress has been made in elucidating these mechanisms, identifying predictive biomarkers for radioresistance remains critical.

STC2, a member of the highly conserved secreted glycoprotein hormone family, is markedly upregulated under stress conditions such as endoplasmic reticulum stress, hypoxia, and nutrient deprivation [5]. Research has demonstrated that STC2 plays a dual role in cancer biology: intracellularly, it modulates stress responses by regulating calcium channel expression or activity, and promotes tumor cell survival and proliferation through metabolic and anti-apoptotic signaling pathways. Extracellularly, it influences the tumor microenvironment via autocrine and paracrine mechanisms, facilitating tumor invasion, metastasis, and immune evasion [6]. STC2 is overexpressed in various cancers, including cervical cancer [7], hepatocellular carcinoma [8], nasopharyngeal carcinoma [9], and glioma [10], and is closely associated with tumor progression, metastasis, and poor prognosis. Furthermore, STC2 has been implicated in radioresistance. For instance, in nasopharyngeal carcinoma [11] and esophageal squamous cell carcinoma [12], high STC2 expression significantly enhances cancer cell resistance to radiotherapy. Furthermore, while STC2 upregulation has been associated with enhanced proliferation, invasion, and metastasis in lung cancer cells [13], its precise role in LUAD and implications for radioresistance and prognosis remain unclear. Therefore, further investigation into the relationship between STC2 and radiation resistance in LUAD will help elucidate its underlying molecular mechanisms and provide novel therapeutic targets to overcome clinical radioresistance.

In summary, while radioresistance is closely associated with therapeutic response, the molecular mechanisms underlying radioresistance in LUAD patients are not fully understood. This study aims to explore the relationship between RRRGs and LUAD, with a focus on elucidating the role of STC2 in LUAD radioresistance and evaluating its potential as a predictive biomarker to enhance the efficacy of radiotherapy in LUAD patients.

Methods

Cell culture and sequencing

The human LUAD cell line A549 was purchased from Peking Union Cell Resource Centre. Cells were cultured in RPMI 1640 medium supplemented with 10% fetal bovine serum (FBS), 100 U/mL penicillin, and 100 U/mL streptomycin (all from Thermo Fisher Scientific, USA) in a humidified incubator at 37 °C with 5% CO₂. The linear accelerator (Meditec Medical Devices, Sweden) was operated at 6 MV X-ray energy for irradiation. The treatment parameters were set as follows: a source skin distance of 100 cm, a radiation field size of 20 × 20 cm², and a dose rate of 200 cGy/min. Cells were irradiated with 2 Gy per fraction, delivered in 30 fractions (5 fractions per week), for a total dose of 60 Gy [14]. Following an additional 24-hour incubation period post-irradiation, cells were washed twice with 1× phosphate-buffered saline (PBS), harvested with 0.25% trypsin, and collected in RNAase-free tubes for RNA extraction. Total RNA was isolated from both irradiated and control cells using a total RNA extraction kit (Tiangen Biochemical Co. Ltd.).

RNA sequencing was subsequently performed by Shanghai Liebing Biomedical Technology Co., Ltd., including RNA quantification, library preparation, clustering, and sequencing.

Transcriptome and clinical data acquisition and collation

Transcriptomic and clinical data for LUAD patients were downloaded from The Cancer Genome Atlas (TCGA, <https://portal.gdc.cancer.gov/>) as a training dataset. The GSE68465 microarray dataset from the Gene Expression Omnibus (GEO, <https://www.ncbi.nlm.nih.gov/geo/>) served as the validation dataset. Cases without sufficient survival information, survival duration of less than 30 days, or lacking pathological staging data were excluded. For genes matched by multiple probes, the probe with the highest expression was selected for further analyses.

Radiation resistance-related genes acquisition

Differentially expressed genes (DEGs) between IR and N-IR cells and between Res and N-Res in TCGA LUAD radiotherapy patients were identified separately using DESeq2 in R software. The criteria for DEGs identification were $|\log_2 \text{fold-change} (\log_2\text{FC})| > 1$ and $p < 0.05$. The intersection of these gene sets was identified as RRRGs, and a Venn diagram was generated using an online tool (<https://bioinformatics.psb.ugent.be/webtools/Venn/>).

GO and KEGG analysis

Functional annotation and pathway enrichment analyses of radio-differential genes were performed using Gene Ontology (GO) and Kyoto Encyclopedia of Genes and Genomes (KEGG) databases. GO annotations were

retrieved from NCBI, UniProt, and Gene Ontology resources. Significant GO categories and KEGG pathways were determined by Fisher's exact test, with a significance threshold of $p < 0.05$.

Consensus clustering analysis

Consensus clustering analysis based on radio-differential genes was conducted using the 'ConsensusClusterPlus' R package, with 1,000 iterations and an 80% resampling rate. The optimal number of clusters (k) was determined using cumulative distribution function (CDF) plots generated by the k-means algorithm, ranging from $k=2$ to $k=6$.

Prognostic model construction and validation

Candidate prognostic genes in the TCGA set were obtained by univariate Cox regression analysis of RRRGs. A Cox proportional risk model with LASSO penalty (iteration = 1000) was used to develop a prognostic signature for RRRGs using the 'glmnet' R package. The risk score was equal to the sum of each gene expression multiplied by the corresponding coefficient. The 'survival' and 'ROC' R packages were employed for survival analyses and time-dependent receiver operating characteristic (ROC) curve analysis, respectively. The 'survival' and 'survminer' R packages were used for Kaplan-Meier survival curves. Intergroup comparisons were performed using Wilcoxon and Kruskal-Wallis tests.

Single-cell analysis validation

In this study, single-cell RNA sequencing data of LUAD and normal lung tissue samples were obtained from the Code Ocean (Single-cell RNA sequencing of human lung adenocarcinomas | Code Ocean) website, and a total of 8 pairs of samples were selected [15]. First, cells and genes included in the study were screened according to the following criteria: 1) Remove cells expressing fewer than 200 genes; 2) Remove genes expressed in fewer than 3 cells; 3) Retain cells with a fluctuating number of expressed genes between 300~5000; 4) Retain cells with a percentage of mitochondrial genes of less than 10%. The data were normalised and PCA downscaled using the standardised 'harmony' method to integrate the different samples and remove batch effects. The FindMarkers function of the Seurat package was used to analyse the differences of each cell group. Ten cell clusters were identified using the Single R package and CellMarker website. (CellMarker2.0). The VlnPlot and DimPlot functions were then used to display the expression of the RRRGs in each cluster and grouped into tumor and normal samples.

Clinical data collection and analysis

Clinical data from LUAD patients undergoing radiotherapy were collected from the First Affiliated Hospital of Xi'an Jiaotong University, approved by the Ethics Committee. Inclusion and exclusion criteria are shown in Fig. 1. Clinical characteristics were analysed using chi-squared and rank-sum tests.

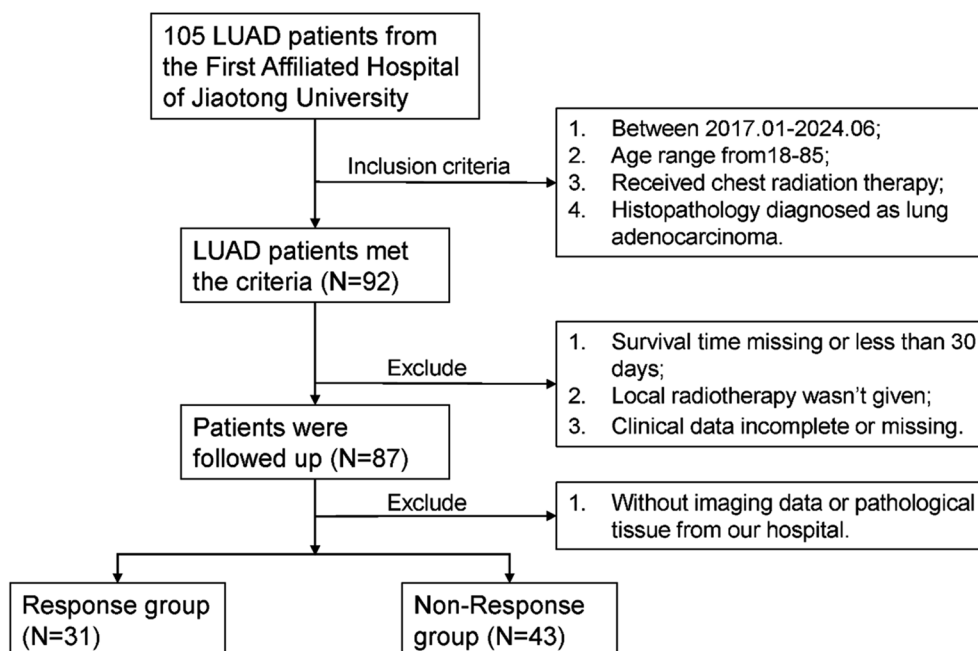


Fig. 1 The flow chart of data collection

IHC staining

Tumor and adjacent normal tissues from LUAD patients undergoing radiotherapy were obtained from the pathology department and the tissues were fixed in 10% formalin, embedded in paraffin and sectioned. The best tissue sections were then selected for dewaxing and standard IHC. IHC was performed according to the standard affinity-biotin method [16]. Finally, desiccation, microscopic examination, image acquisition and analysis were performed. Antibody information was obtained from Immunoway: STC2 (dilution: 1:100). We randomly selected five microscopic fields of view of tumor tissue and scored all samples using a semi-quantitative system that takes into account the intensity and proportion of staining. Stained sections were divided into high and low expression groups based on the intensity and extent of staining.

Cell transfection

The siRNA used to knockdown STC2 was provided by Bioengineering (Shanghai) Co, and the sequence is shown in Supplementary Table S1. Cells were inoculated into 6-well plates at a concentration of 1×10^6 cells per well and cultured for 24 h. When cell fusion reached 70–80%, cell transplantation was performed using Lipofectamine 3000 (Thermo Fisher Scientific, USA). The transfection solution was added to the cells drop by drop. Transfection efficiency was assessed by qRT-PCR and Western blotting after 48 and 72 h, respectively.

Western blotting analysis

Total proteins were extracted using RIPA lysis buffer (Sigma, USA). The lysates were collected and centrifuged at 12,000 rpm for 20 min at 4 °C. Proteins were separated by 10% SDS-PAGE electrophoresis (Abe Medical Devices Trading (Shanghai) Co., Ltd.) and subsequently transferred to a PVDF membrane (Burroughs Lifecare Medical Products (Shanghai) Co., Ltd.). The membrane was incubated with primary antibody at 4 °C overnight, followed by TBST buffer washes (Solebrite Technology Co., Ltd.). After washing, the membrane was incubated with STC2 secondary antibody at room temperature. The luminescent solution was prepared according to the manufacturer's instructions of the ECL kit (Shanghai Tannen Life Science Co., Ltd.). Make the luminescent solution in full contact with the membrane, and transfer the membrane into the luminescence instrument for luminescence to visualise the protein bands.

qRT-PCR

Total RNA was extracted from cultured cells using TRIzol reagent (TaKaRa, Dalian, China), and RNA concentrations were measured using a Nanodrop ND-2000 spectrophotometer (absorbance at 260/280 nm). RT-PCR was performed using Hieff qPCR SYBR Green Master

Mix (No Rox; Yeasen Biotechnology, Shanghai, China) under the following cycling conditions: initial denaturation at 95 °C for 2 min, followed by 40 cycles of denaturation at 95 °C for 15 s, annealing at 60 °C for 30 s, and extension at 72 °C for 30 s. RNA expression data were normalized to GAPDH and analyzed using the $2^{(-\Delta\Delta Ct)}$ method. All primer sequences are provided in Supplementary Table S1, and were synthesized by Bioengineering (Shanghai) Co., Ltd.

Colony formation assay

Irradiated A549 cells in the logarithmic growth phase were seeded into 6-well plates at gradient densities, and STC2 was knocked down using siRNA. The siSTC2 and NC group cells were irradiated with doses of 0, 2, 4, 6, and 8 Gy, then cultured for 10–14 days post-irradiation. Cells were fixed with 2 mL of 4% paraformaldehyde (Shaanxi Zhonghui Hecai Biomedical Technology Co., Ltd.) per well for 15 min and stained with crystal violet (Jining Hongming Chemical Reagent Co., Ltd.) for 20 min. Clonal colonies were counted after air drying, with colonies containing more than 50 cells considered positive. The NC group served as a control for assessing changes in clonogenic survival. Survival curves were fitted using the single-hit multi-target model.

CCK8 assay

Cell proliferation was evaluated using the Cell Counting Kit-8 (CCK-8) (Shanghai Taosu Biochemical Technology Co., Ltd.). Fresh cell suspensions were prepared at a concentration of 40,000 cells/mL. Each well of a 48-well plate received 200 μ L of the cell suspension, with five replicate wells per group. After 24 h, 200 μ L of prepared CCK8 reagent was added to each well. The 48-well plates were assessed every 24 h, shaken gently, and absorbance was measured using a spectrophotometer. Optical density (OD) values, indicating the number of viable cells, were recorded at 0, 24, 48, and 72 h, and the experiments were repeated three times.

Statistical analysis

Clinical data were analyzed using univariate Cox regression analysis, and Kaplan-Meier (KM) analysis was used to generate survival curves. Differences in categorical variables were assessed by the chi-squared test, while continuous variables between two groups were compared using the t-test. Comparisons involving more than two groups were performed using one-way ANOVA. Statistical analyses were conducted using SPSS (version 24), R software (version 4.3.2), and GraphPad Prism 8.0 software. Statistical significance was defined as $p < 0.05$.

Results

Radioresistant LUAD cells constructed and analysed after sequencing

RNA sequencing was conducted to identify DEGs between IR and N-IR LUAD A549 cells. The establishment of a radio-resistant LUAD A549 cell line via cumulative irradiation is depicted in Fig. 2A. A total of 770 significantly DEGs were identified ($p < 0.05$), including 540 upregulated and 230 downregulated genes in IR cells compared to N-IR controls. The complete gene list is provided in Supplementary Table S2. The MA-plot and heatmap of these DEGs are shown in Fig. 2B

and C, respectively. To elucidate the molecular mechanisms underlying radiotherapy resistance, we performed GO and KEGG pathway enrichment analyses on DEGs between radiation-resistant and control samples. GO enrichment analysis revealed that the DEGs were significantly enriched in biological processes such as extracellular matrix organization, cell adhesion, and cell cycle (Fig. 1D). KEGG pathway analysis further demonstrated that the DEGs were primarily involved in key pathways including the cell cycle, ECM-receptor interaction, PI3K-Akt signaling, and cellular senescence (Fig. 1E). Specifically, cell cycle regulation is closely associated with cell

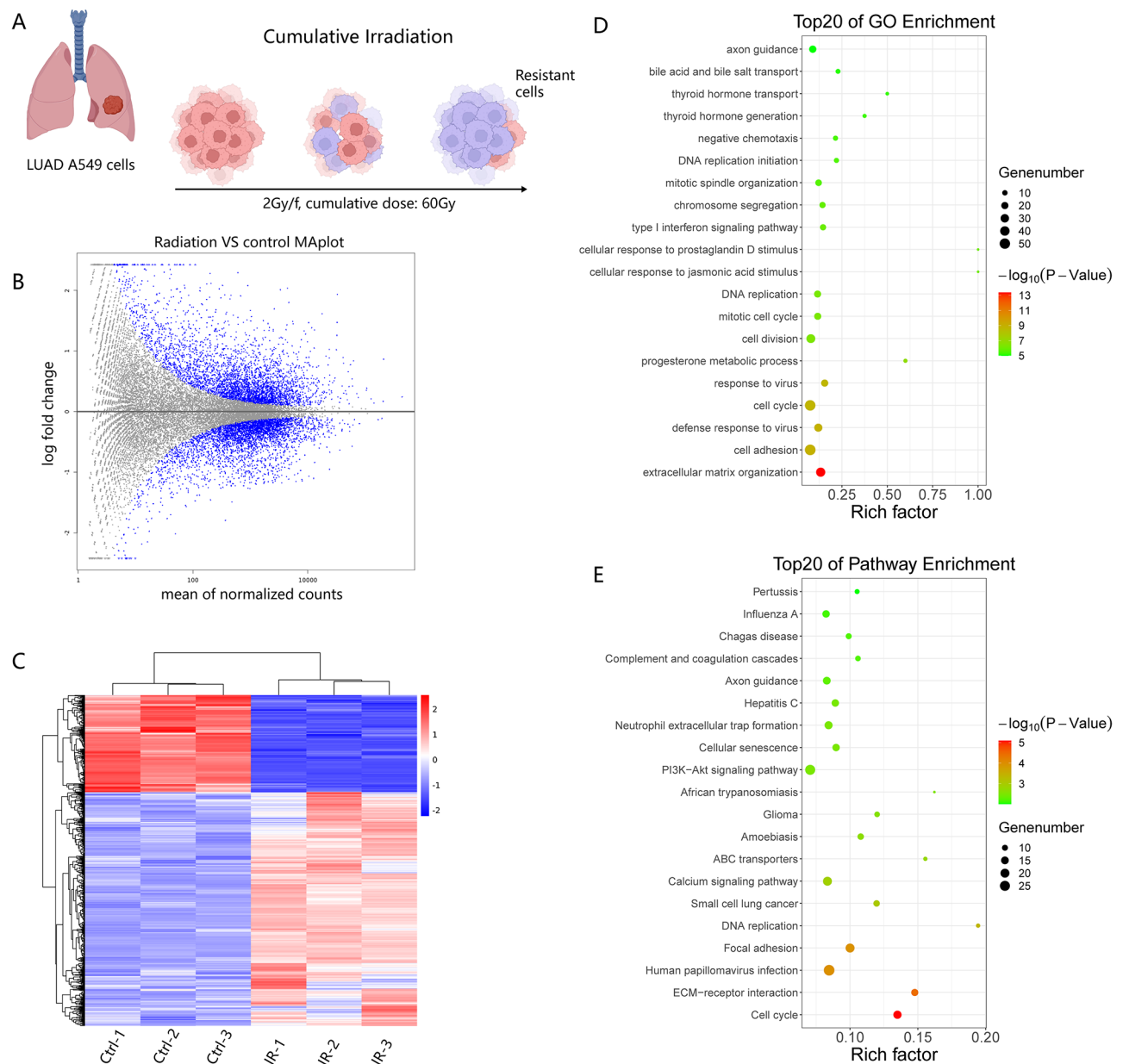


Fig. 2 The radio-differential genes acquisition. **(A)** Radio-resistant cell line was established by cumulative irradiation. **(B)** and **(C)** radio-differential genes MA-plot plots and heatmaps. Differential genes GO and KEGG pathway bubble plots are shown in **(D)** and **(E)**

proliferation and DNA damage repair, cell adhesion processes influence tumor cell invasion and metastasis, and the PI3K-Akt signaling pathway modulates cell survival, proliferation, and metabolism. These findings imply that LUAD cells may acquire radioresistance by modulating processes related to cell cycle control, extracellular matrix composition, and cellular adhesion, contributing to enhanced survival following irradiation.

TCGA and GEO LUAD data collation and differential genes acquisition

RNA expression and clinical information of LUAD were downloaded from the TCGA database, and the genes that were all expressed in 50% of the samples were selected by matching the expression information with the clinical information. We obtained a total of 444 patients' clinical information and 20,609 genes. The TCGA clinical data were collated to exclude cases with no survival information and survival time less than 30 days and no pathological staging. Finally, 104 LUAD patients who received radiotherapy were obtained, of which 85 cases had prognostic information (Supplementary Table S3). Meanwhile, the genetic and clinical data of 65 LUAD patients

receiving radiotherapy was obtained from the GSE68465 for validation. Consistent clustering analysis based on radio-differential genes was performed on LUAD patients receiving radiotherapy in TCGA. The results demonstrated that LUAD patients could be effectively classified into two distinct groups using these radio-differential genes (Fig. 3A and B), with a statistically significant difference in survival outcomes between the groups (Fig. 3C). Immune cell infiltration analysis revealed significant differences in the infiltration levels of T cells and macrophages between the two clusters (Fig. 3D).

Construction and validation of a prognostic model based on RRRGs

We considered patients with efficacy CR and PR as the Res group and SD and PD patients as the N-Res group. Differential gene analysis yielded 1242 prognostic-differential genes ($P < 0.05$), with 315 upregulated and 927 downregulated genes. The Fig. 4A shows the volcano plot of the DEGs. Radio-differential genes and prognostic-differential genes were intersected to obtain 34 genes as RRRGs, which were shown in Venn diagrams (Fig. 4B). Univariate Cox regression analysis identified 6 significant

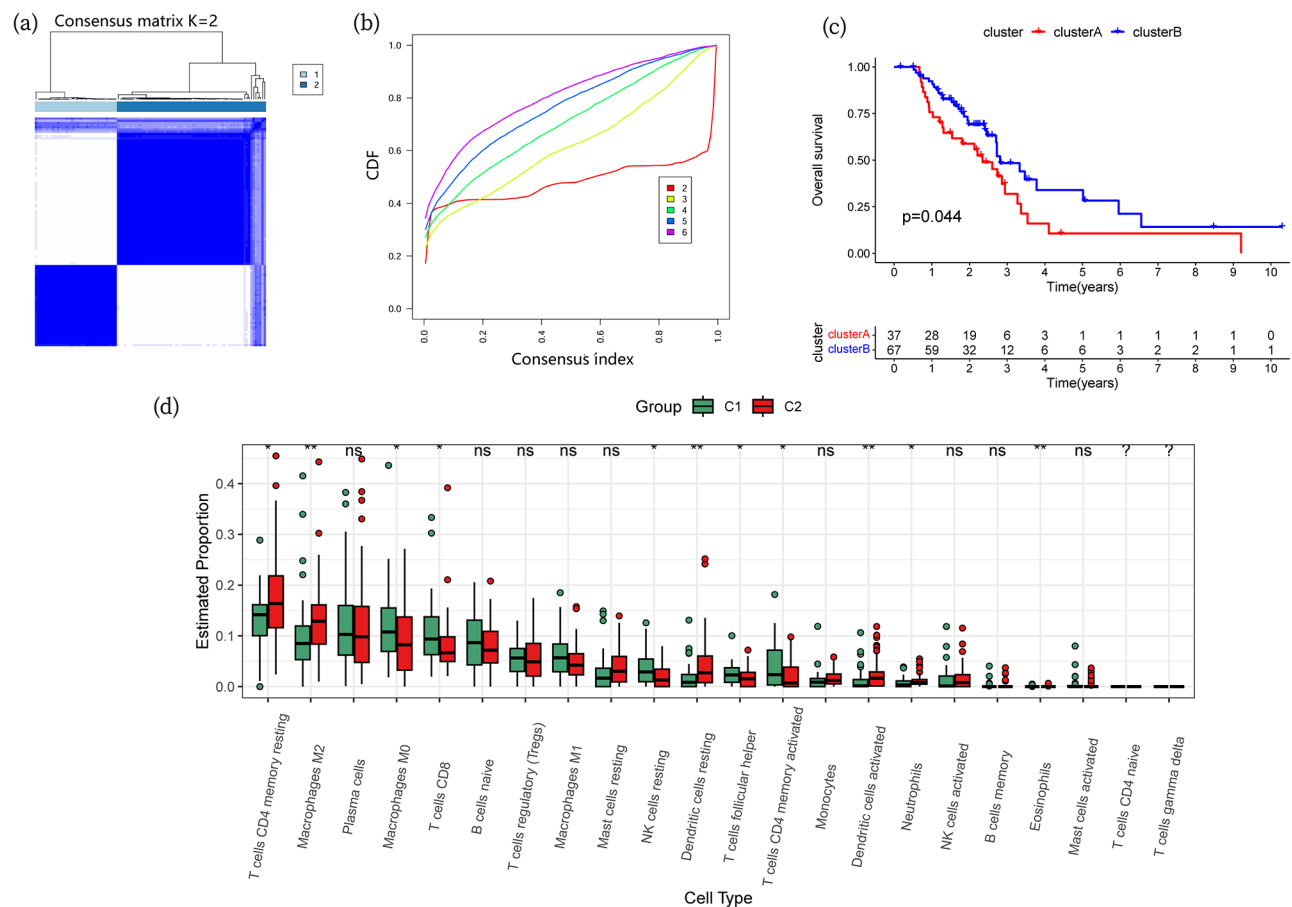


Fig. 3 Consensus cluster analysis based on radio-differential genes for LUAD patients receiving radiotherapy in TCGA. (A) (B) Consensus matrix works best with cluster number (k)=2. (C) Kaplan-Meier curve showing survival differences between subtypes. (D) Two-cluster immune cell infiltration analysis

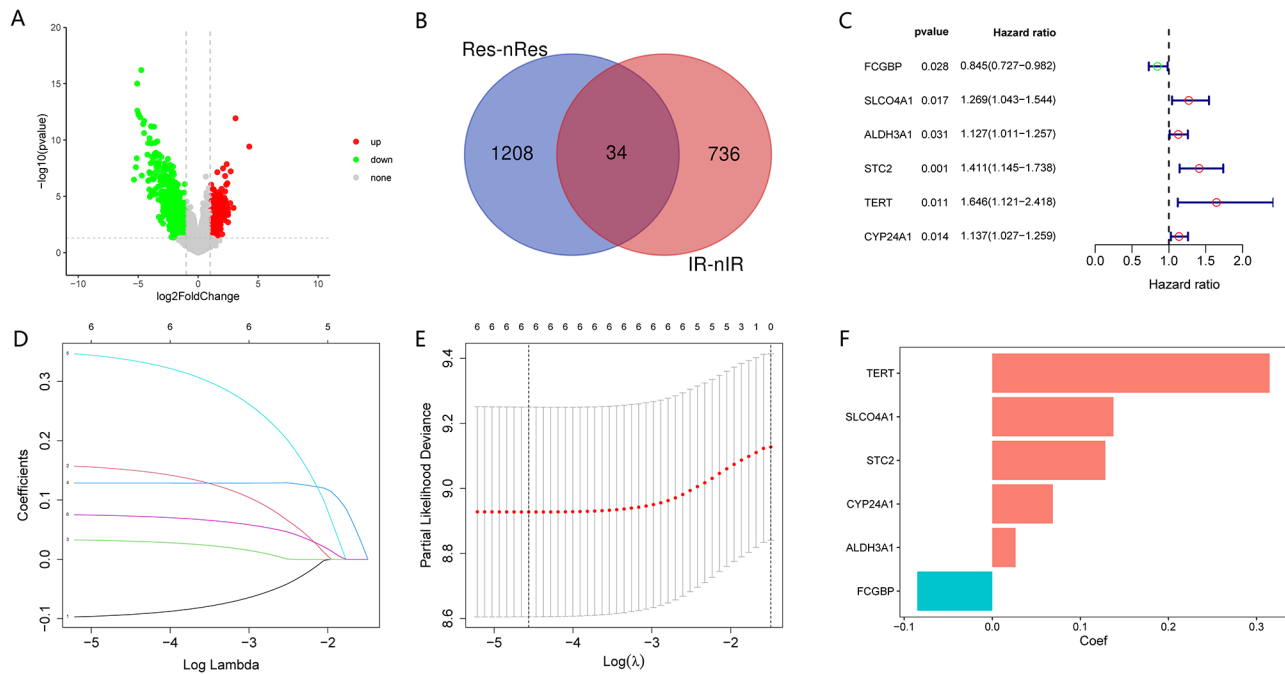


Fig. 4 Screening of signature genes and prognostic model construction. **(A)** Volcano plot of prognostic-differential genes obtained from the analysis of LUAD patient differences between Res and N-Res in TCGA. **(B)** Venn diagram of prognostic-differential genes versus radio-differential genes. **(C)** Forest plot showing the results of univariate Cox regression analysis. **(D)** LASSO-Cox regression analysis based on RRRGs. **(E)** LASSO coefficients for RRRGs in LUAD. **(F)** Histogram of LASSO genes coefficients

RRRGs (FCGBP, SLCO4A1, ALDH3A1, STC2, TERT, CYP24A1; Fig. 4C). A prognostic model was developed using LASSO-Cox regression based on these 6 RRRGs, resulting in a predictive risk score formula (Fig. 4D and E). The risk score was quantified using the following formula: $(-0.0851253128228653 \times \text{mRNA expression level of FCGBP}) + (0.13759557595724 \times \text{mRNA expression level of SLCO4A1}) + (0.026399137254701 \times \text{mRNA expression level of ALDH3A1}) + (0.128449154347007 \times \text{mRNA expression level of STC2}) + (0.314899482100938 \times \text{mRNA expression level of TERT}) + (0.0687707796459586 \times \text{mRNA expression level of CYP24A1})$. The histogram of LASSO gene coefficient is shown in Fig. 4F. The risk scores of all patients were calculated according to the formula, and LUAD patients receiving radiotherapy were divided into high-risk and low-risk groups using the median risk score as the cut-off value.

We used the same formula to calculate risk scores for LUAD patients in the GEO cohort to validate the prognostic prediction capability of the model. Kaplan-Meier survival curves demonstrated that OS was significantly lower in the high-risk group compared to the low-risk group in both the TCGA ($p < 0.01$, Fig. 5A) and GEO cohorts ($p = 0.006$, Fig. 5B). To evaluate the prognostic efficacy, we applied time-dependent ROC curve analysis. The area under the ROC curve (AUC) for predicting 1-, 3-, and 4-year survival was 0.687, 0.764, and 0.840, respectively, in the TCGA group (Fig. 5C). Consistent

results were obtained in the GEO cohort, with AUC values of 0.764, 0.682, and 0.662, respectively (Fig. 5D). The distribution of risk scores, survival statuses, and heat-maps illustrating the expression patterns of the 6 RRRGs are shown in Fig. 5E and F.

Association of STC2 expression with clinical data of LUAD patients in TCGA and GEO

We further investigated the relationship between high and low expression levels of each RRRGs and patient survival. High expression of FCGBP was associated with improved survival ($p = 0.015$), whereas elevated expression of the remaining five genes was associated with poorer prognosis ($p < 0.05$) (Fig. 6A-F). In the univariate Cox regression analysis, STC2 demonstrated the most significant association with prognosis in LUAD patients ($p = 0.001$) and exhibited a relatively high hazard ratio (HR = 1.411), suggesting its potential biological importance in LUAD progression. ROC curve analysis of the prognostic performance among all RRRGs revealed STC2 as the top-performing biomarker (AUC = 0.661, Supplementary Fig. 1). Based on these findings, STC2 was selected as the primary candidate gene for further investigation to validate its role in radioresistance and clinical outcomes in LUAD. Subsequently, we analyzed the relationship between STC2 expression and radiotherapy efficacy in LUAD patients. Our analysis revealed no significant correlation between STC2 expression and

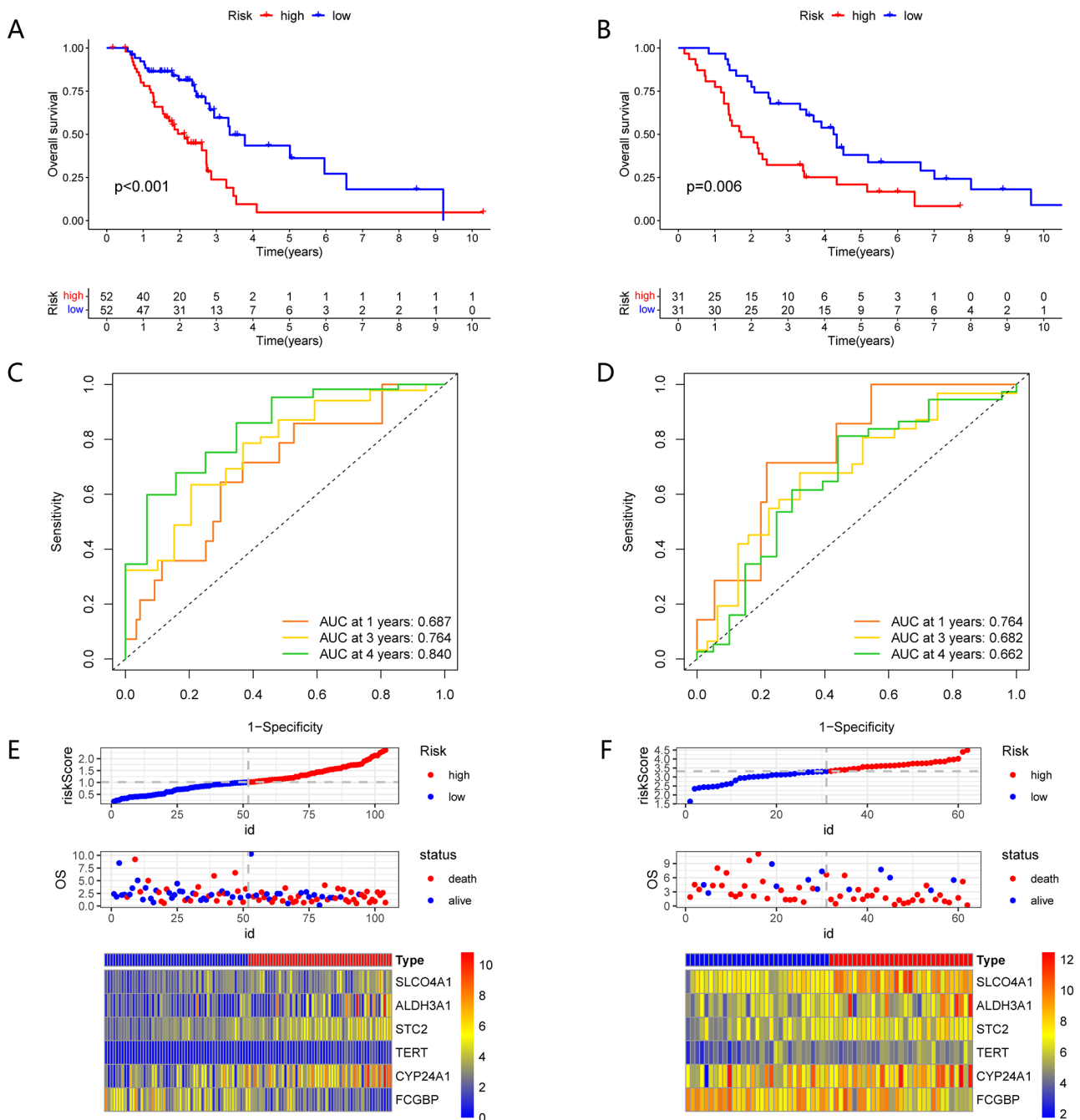


Fig. 5 Validation of the risk model. Kaplan-Meier survival curves show differences in OS between TCGA (A) and GEO (B) high and low risk groups. Predicted TCGA cohort (C) and GEO cohort (D) time-dependent curves ROC showed good results. (E) and (F) Distribution of survival statuses and heatmaps for RRRGs

patient age, gender or tumor staging (Fig. 6G-L). However, within gender subgroups, STC2 expression was significantly higher in females than in males ($p = 0.016$) (Fig. 6H). Further analysis of the TCGA database demonstrated that STC2 expression was significantly elevated in tumor tissues compared to adjacent non-tumor tissues (Fig. 6M, $p = 0.0094$). Additionally, a significant difference in STC2 expression was observed between Res and N-Res

groups, with higher expression levels found in the N-Res group (Fig. 6N, $p = 0.011$). Survival analysis of LUAD patients receiving radiotherapy in the TCGA database confirmed that high STC2 expression correlated significantly with poor prognosis (Fig. 6E, $p = 0.0067$). Although a similar trend was observed in the GSE68465 dataset, this difference was not statistically significant, potentially due to the smaller sample size (Fig. 6O, $p = 0.082$).

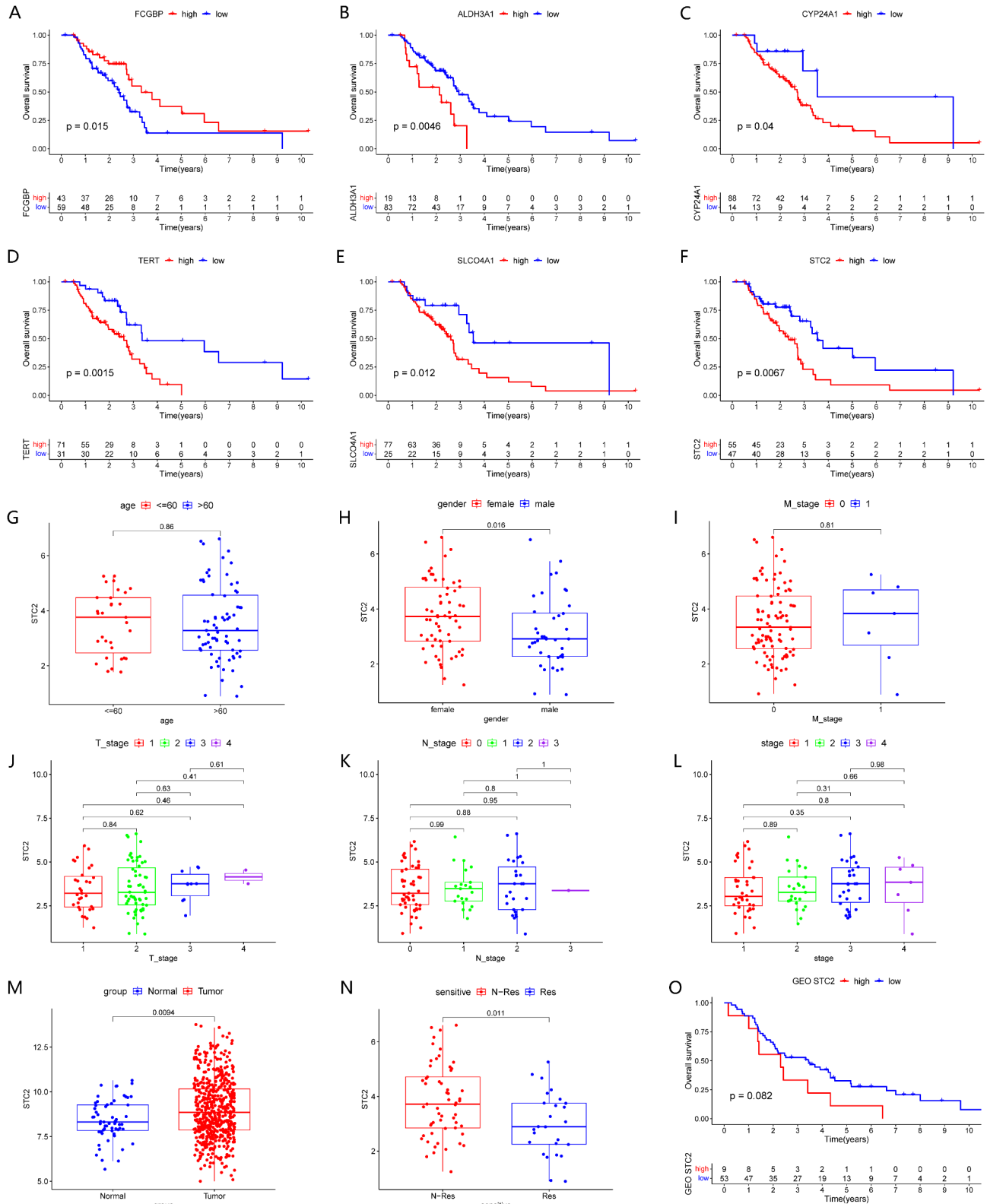


Fig. 6 Relationship between the expression of RRRGs and TCGA and GEO clinical data. **(A)-(F)** K-M curves of the expression of RRRGs versus survival in LUAD patients; Box plots of age **(G)**, gender **(H)**, M **(I)**, T **(J)**, N **(K)** and stage **(L)** grouped according to high and low STC2 expression. **(M)** Box plots of the comparison of the expression of STC2 in tumor and normal tissues. **(N)** Box plots of the comparison of the expression of STC2 in the efficacy Res group and N-Res group. **(O)** KM curve of STC2 versus survival validated by GEO data

Expression of 6 RRRGs in LUAD single-cell sequencing data

Next, we analysed 8 pairs of single-cell sequencing samples from LUAD and corresponding normal tissues obtained from the Code Ocean website. After filtering cells and genes and performing PCA dimensionality reduction, the samples showed an even distribution (Supplementary Fig. S2A). Finally, 52,677 cells were obtained for subsequent analyses. The Supplementary Fig. 2A shows the distribution of all samples and the initially identified cell subpopulations. Based on the differentially expressed genes of each subpopulation and cell-type-specific marker genes, we finally identified 10 distinct cell populations (Supplementary Fig. S2B): 'AT1-cell', 'AT2-cell', 'B-cell', 'Ciliated airway epithelial', 'Cycling cell', 'Mast cell', 'Myeloid cell', 'Plasma cell', 'Stromal cell', and 'T-cell'. The expressions of RRRGs in each cell population are shown in umap and bar plots (Supplementary Fig. S2C and D), revealing that FCGBP, SLCO4A1, ALDH3A1, STC2 were expressed in both AT1 and AT2 cell subpopulations, while CYP24A1 was primarily expressed in the AT2 cell subpopulation. TERT showed low expression across all cell types. Subsequently, samples were categorized into tumor and normal groups to examine STC2 expression differences between these groups (Supplementary Fig. S2E and F). STC2 expression was higher in normal tissues compared to tumor tissues within AT1 cells. Conversely, STC2 expression was significantly higher in tumor tissues relative to normal tissues within AT2 cells. This may be related to the fact that AT2 cells are more prone to accumulating mutations and undergoing malignant transformation compared to AT1 cells.

Expression of STC2 in LUAD tissues

To further validate the relationship between STC2 expression and LUAD patients, clinical information and pathological tissues from LUAD patients who received radiotherapy at the First Affiliated Hospital of Xi'an Jiaotong University were collected and followed up. According to the defined inclusion and exclusion criteria, 74 LUAD patients receiving radiotherapy were enrolled. Patient treatment efficacy was evaluated according to RECIST 1.1 criteria, with 31 patients classified in the Res group and 43 in the N-Res group. Baseline clinical characteristics are detailed in Supplementary Table S4, and the analysis indicated no significant differences in gender, age, stage, TNM stage, or smoking history between the Res and N-Res groups ($p > 0.05$).

Subsequently, IHC staining was performed on the 74 collected LUAD pathological sections to assess STC2 protein expression. Positive staining intensities (colorless, yellowish, brown, and tan) were scored as 0, 1, 2, and 3, respectively. Additionally, the proportions of positively stained cells were categorized as <25%, 25–50%, 51–75%, and >75%, scored as 1, 2, 3, and 4, respectively. The final

IHC staining score, ranging from 0 to 12, was calculated by multiplying the intensity and proportion scores, with scores of 0–6 indicating "low expression" and 7–12 indicating "high expression." IHC results demonstrated that STC2 expression was higher in the N-Res group than in the Res group and lowest in normal tissues (Fig. 7A). Further analysis revealed that STC2 expression was significantly higher in the N-Res group compared to the Res group ($\chi^2 = 5.737$, $p = 0.017$), and higher in tumor tissues compared to adjacent normal tissues ($\chi^2 = 5.286$, $p = 0.021$) (Supplementary Table S5). Survival analysis showed patients with low STC2 expression had significantly longer OS and progression-free survival (PFS) compared to those with high STC2 expression, indicating that elevated STC2 expression correlates with poorer prognosis in LUAD patients (Fig. 7B and C).

Western blotting to verify STC2 expression in N-IR and IR cells

We performed Western blotting analysis on IR and N-IR A549 cells after protein extraction to verify the protein expression of STC2. The results demonstrated significantly higher STC2 expression in A549 cells irradiated with 60 Gy/30 fractions compared to the parental non-irradiated cells (Fig. 7D and E, $p < 0.01$). These findings suggest that STC2 may play a role in mediating radioresistance.

Knockdown of STC2 increases radiosensitivity of LUAD cells

To further clarify the effect of STC2 on tumor radiosensitivity, we conducted a colony formation assay using A549 cells. Initially, the A549 cells were divided into two groups: the experimental group, in which STC2 expression was knocked down using siSTC2, and the NC group, which was left untreated. The knockdown efficiency was confirmed through Western blotting and qRT-PCR, demonstrating that siRNA sequence 2 had the highest knockdown efficiency (Fig. 8A–C). Thus, sequence 2 was selected for subsequent experiments. Following successful STC2 knockdown, both siSTC2 and NC groups were irradiated with graded doses of 0, 2, 4, 6, and 8 Gy, and the colonies were fixed and stained after two weeks. Comparing the two groups, we found that the colony numbers were significantly lower in the siSTC2 group compared to the NC group (Fig. 8D), with the surviving fraction decreasing as irradiation doses increased. Using the colony formation rates per well from Fig. 8D, we fitted the survival curves using the single-hit multi-target model: $SF = 1 - (1 - e^{-kD})^N$. Figure 8E shows that the colony formation rate in the siSTC2 group was significantly lower than in the NC group, indicating enhanced radiosensitivity ($p < 0.05$). These findings suggest that knocking down STC2 expression increases the radiosensitivity of LUAD cells.

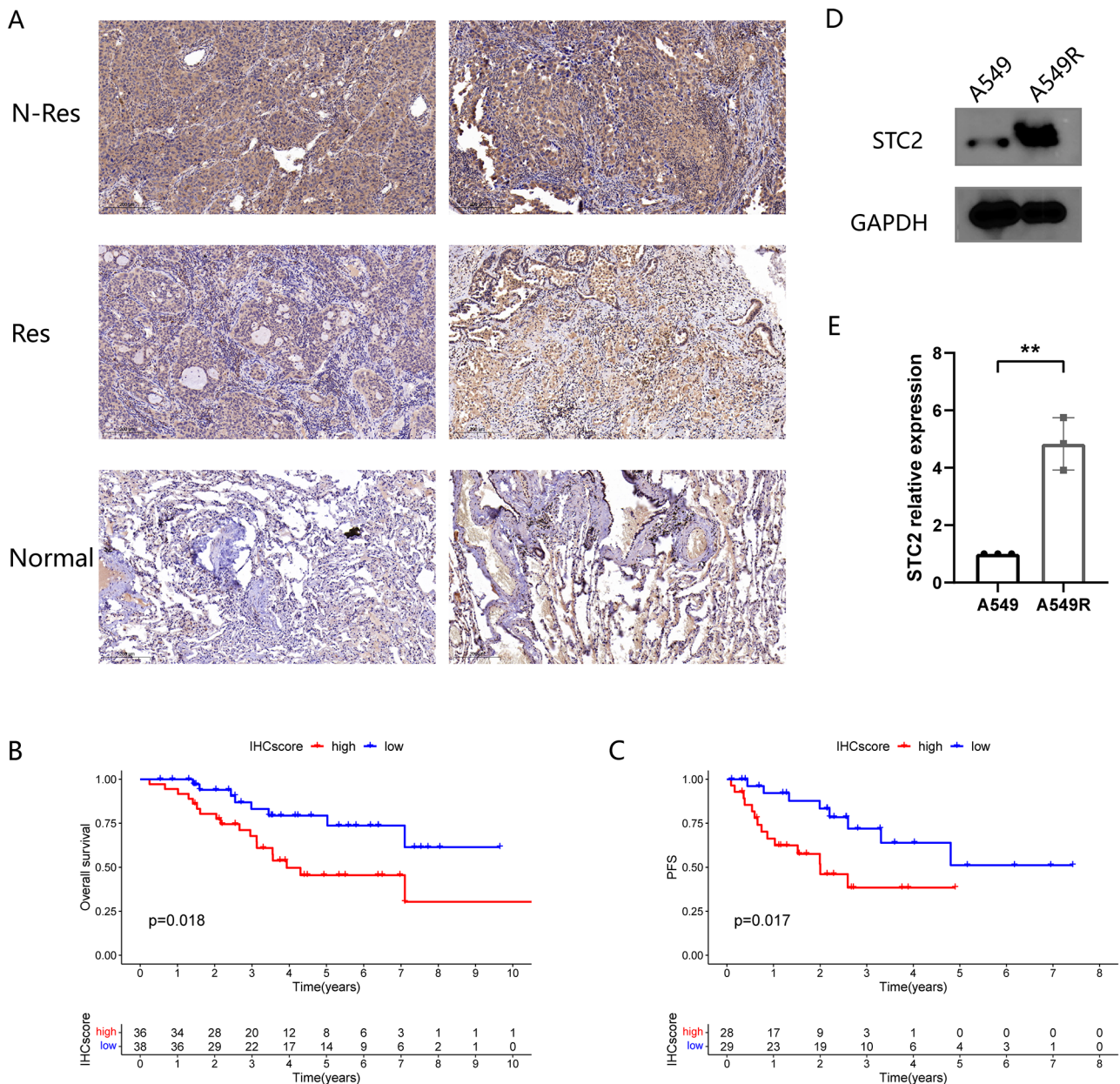


Fig. 7 IHC and Western blotting demonstrating STC2 expression. **(A)** Representative graphs of IHC of STC2 in each group of lung tissues. Survival analysis curves of STC2 expression versus OS **(B)** and PFS **(C)** in LUAD patients receiving radiotherapy. **(D)** and **(E)** Western blotting demonstrating the expression level of STC2 before and after IR of A549 cells (* $p < 0.05$, ** $p < 0.01$)

Effect of STC2 on the proliferative capacity of A549 cells

To evaluate the proliferation ability of A549 cells in the NC and siSTC2 groups, we utilized the CCK-8 assay, measuring absorbance at 450 nm at 0, 24, 48, and 72 h after seeding cells into 48-well plates. Absorbance readings were taken every 30 min following the addition of the CCK-8 reagent, and readings at 1.5 h after reagent addition were identified as optimal (absorbance < 2). The results, as illustrated in Fig. 8F, indicated no significant difference in proliferation between the two groups within the first 24 h post-STC2 knockdown. However,

from 24 h onwards, a significant difference emerged, with the proliferation rate of cells in the siSTC2 group notably lower than that of the NC group ($p < 0.05$). The difference between siSTC2 group and NC group was most significant at 48 h. These findings demonstrate that STC2 knockdown significantly reduces A549 cell proliferation, suggesting a role for STC2 in promoting cell proliferation.

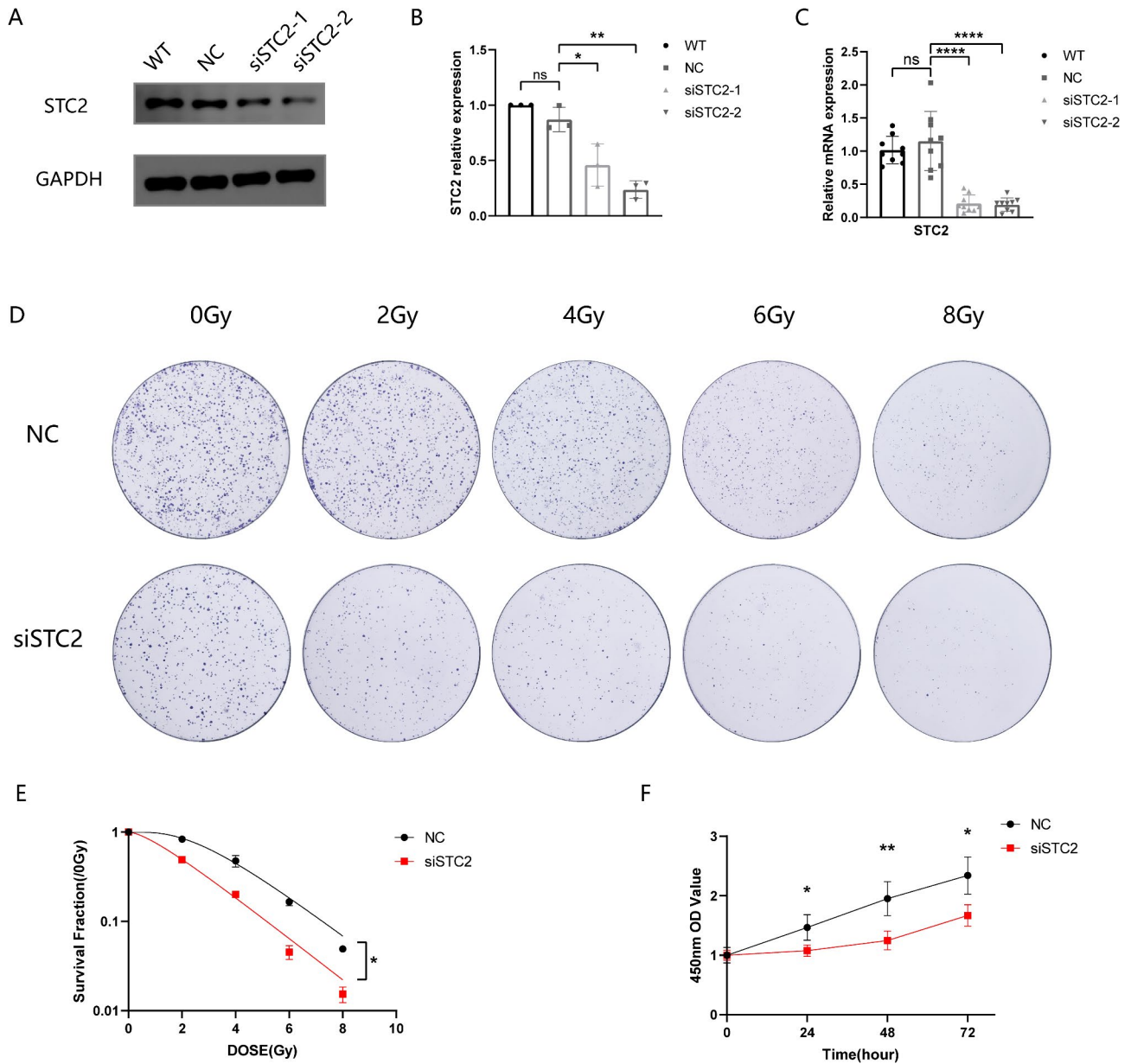


Fig. 8 CCK8 and cloning assays to detect proliferative capacity and clone formation of LUAD cells. Western blotting (A), (B) and qRT-PCR (C) validation of the knockdown effect of STC2. (D) Representative images of clone formation in A549 cells irradiated with different doses of X-rays. (E) Survival based on the single-hit multi-target model fit to the fraction curves. (F) Line chart of cell proliferative capacity before and after STC2 knockdown (* $P < 0.05$, ** $P < 0.01$, *** $P < 0.001$, ns: no statistical difference)

Discussion

Lung cancer remains one of the most lethal malignancies worldwide, with LUAD representing the predominant histological subtype [3]. Despite considerable advancements in radiotherapy, radioresistance continues to significantly limit treatment efficacy and patient outcomes. Therefore, understanding the underlying mechanisms of radiation resistance is essential for improving treatment strategies. In this study, we employed an integrative approach combining RNA sequencing, bioinformatics analysis, and experimental validation to identify STC2 as

a key gene associated with LUAD radioresistance. Our findings demonstrate that STC2 not only plays a significant role in mediating radioresistance but also correlates closely with poor prognosis in LUAD patients.

Radioresistance is a multifaceted phenomenon resulting from intricate interactions among genetic, epigenetic, and tumor microenvironment factors. To investigate the molecular mechanisms and identify key drivers of radioresistance, we established a radioresistant A549 LUAD cell line using cumulative irradiation, a method previously validated by Pustovalova et al. [14], Alhaddad et al.

[17]. This approach simulates clinical fractionated radiotherapy by exposing cells to repeated low-dose irradiation, thereby selecting for a radioresistant subpopulation. Pustovalova et al. showed that after 60 Gy/30 fractions, radio-resistant sublines of A549 and H1299 cells exhibited significant gene expression changes and pathway activation differences [14], particularly those related to DNA repair, cell cycle regulation, and the immune microenvironment. We also selected 60 Gy/30 fractions irradiation regimen, and sequenced the irradiated cells to screen out the RRRGs with research value. Gene GO and KEGG analyses further revealed that RRRGs were significantly enriched in biological processes such as cell cycle regulation, cell adhesion, extracellular matrix organization, PI3K-Akt signaling, and cellular senescence. These results provide new insights into the molecular mechanisms of radiotherapy resistance and may provide powerful directions for our subsequent pathway studies.

Currently, identifying RRRGs and constructing prognostic models provide promising approaches for the individualized management of lung cancer patients. For instance, Li et al. identified telomere-related genes associated with radioresistance using data from TCGA and GEO databases [18], while Chen et al. developed an 8-gene prognostic risk score model [19]. We constructed a predictive model using LASSO-Cox regression based on 6 RRRGs, including STC2. The area under the ROC curve (AUC) was 0.687, 0.764 and 0.840, respectively, for predicting 1-year, 3-year and 4-year survival. Compared with Li et al.'s (1-year, 3-year, and 5-year AUC of 0.665, 0.681, and 0.630, respectively) and Chen et al.'s (1-year, 3-year, and 5-year AUC of 0.676, 0.692, and 0.614, respectively), our model significantly outperforms other models in survival prediction and demonstrating higher prediction accuracy. Nonetheless, due to the limited sample sizes in publicly available databases, especially concerning long-term survival data, further validation in larger patient cohorts is warranted to confirm the robustness and clinical applicability of our model.

Our study identifies STC2 as a pivotal gene in LUAD radioresistance. STC2 expression was significantly upregulated in LUAD tissues and correlated with poor prognosis and reduced radiosensitivity. These findings align with previous studies on other radioresistance markers in LUAD, such as YAP/TEAD4/NRP1 and APE1 [20], which promote radioresistance through enhanced DNA repair and survival pathways. Additionally, long non-coding RNA CCAT1 has been reported to contribute to LUAD radioresistance by modulating cell proliferation, migration, and apoptosis, as well as influencing pathways like G2M checkpoint and mTORC1 signaling [21]. However, unlike these markers, STC2 appears to modulate calcium homeostasis and cellular stress responses, offering a unique therapeutic target. Based on the GO and

KEGG results and the biological functions of STC2, we hypothesize that STC2 may influence radioresistance in LUAD cells by affecting DNA damage repair, regulating the cell cycle, and modulating cellular stress responses. This hypothesis requires further experimental validation. Moreover, comparative analysis with established radioresistance-related genes in lung cancer revealed that STC2 (AUC=0.661) demonstrated comparable predictive performance to ANGPTL4 (AUC=0.664) [22], while surpassing other known biomarkers, including FBXO22 (AUC=0.587) [23], PKMYT1 (AUC=0.64) [24], and HSD17B6 (AUC=0.602) [25]. The ROC curves are shown in Supplementary Fig. 3. These findings validate the clinical potential of STC2 as a predictive marker for radiotherapy response in LUAD. Importantly, our results not only support the prognostic value of STC2 but also highlight its therapeutic potential as a novel target for radioresistant LUAD. In addition, the role of STC2 in radioresistance has been reported in a few cancers, such as esophageal squamous cell carcinoma, where STC2 induces radioresistance by activating PRMT5 to promote DNA damage repair (DDR) and inhibit ferroptosis [12]. Similarly, in cervical cancer [26] and nasopharyngeal carcinoma [11], overexpression of STC2 is closely associated with tumor progression and radioresistance. Yet, the relationship between STC2 and LUAD radioresistance remained unexplored until this study. We demonstrated for the first time that STC2 expression is significantly upregulated in radioresistant LUAD A549 cells, and its knockdown markedly enhances cellular radiosensitivity. While providing strong evidence for the role of STC2 in LUAD radiological resistance, the underlying mechanism remains to be fully elucidated. Further research is needed to comprehensively explore the precise signaling pathways and interactions through which STC2 contributes to radioresistance. Such studies could facilitate the development of targeted therapeutic strategies.

In conclusion, our study identifies STC2 as a key driver of radioresistance in LUAD and establishes a robust prognostic model based on RRRGs. STC2 overexpression is associated with poor prognosis, and its knockdown significantly reduces clonogenic survival in irradiated A549 cells, confirming its role in radioresistance. Future research should focus on unraveling the molecular mechanisms by which STC2 mediates radioresistance and exploring its therapeutic potential in combination with existing radiotherapy regimens to improve outcomes for LUAD patients.

Conclusion

In summary, our findings highlight STC2 as a critical gene of LUAD radioresistance and an effective prognostic biomarker. The prognostic model based on RRRGs demonstrates strong predictive power, offering a valuable

tool for personalized treatment strategies. Future investigations should further elucidate the detailed molecular mechanisms of *STC2* in radioresistance and validate its clinical applicability.

Supplementary Information

The online version contains supplementary material available at <https://doi.org/10.1186/s12935-025-03783-1>.

Supplementary Table S1: *STC2* small interfering RNA sequence and qRT-PCR primer sequence

Supplementary Table S2: The complete list of radio-differential genes

Supplementary Table S3: Comparison of clinical features between the efficacy subgroups of TCGA LUAD patients

Supplementary Table S4: Comparison of clinical features between the therapeutic groups of LUAD patients in our hospital

Supplementary Table S5: Expression of *STC2* in LUAD tissues and adjacent normal tissues with different prognosis

Supplementary Fig. 1: ROC curve analysis comparing the prognostic performance of 6 RRRGs

Supplementary Fig. 2: Expression of RRRGs in single-cell sequencing of LUAD. (A) Filtered umap plots, coloured by samples or sub-clusters; (B) Annotated umap plots; (C) and (D) expression of RRRGs in each cell population; *STC2* expression in normal and tumor samples of each cell population is shown in (E) and (F)

Supplementary Fig. 3: ROC curve analysis comparing the prognostic predictive value of *STC2* with other known LUAD radioresistance markers

Acknowledgements

We are grateful to the first affiliated hospital of Xi'an Jiaotong University for providing laboratory and LUAD tissues. We would like to thank Professor Shaomin Che for her funding support. We thank all contributors to the TCGA and GEO database. We thank the BioRender web to make the Fig. 1 A. We also thank developers of the R tool and the research team members of Professor Zhang from the first affiliated hospital of Xi'an Jiaotong University.

Author contributions

Drs Li and Zhang had full access to all of the data in the study and took responsibility for the integrity of the data and the accuracy of the data analysis. Y.W. and Y.S. as the co-first author, performed the research analysis and experiment. M.H., Y.W. and B.H. participated in the design of the study. W.H. Participated in joint data collection. M.Z. reviewed the pathological slides of LUAD.

Funding

This research was funded by the Natural Science Basic Research Program of Shaanxi (Program No. 2022JM-462).

Data availability

No datasets were generated or analysed during the current study.

Declarations

Ethics approval and consent to participate

All procedures performed in studies involving human participants were in accordance with the ethical standards of the institutional and national research committee and with the 1964 Helsinki declaration and its later amendments. The project was approved by the ethics committee of the first affiliated hospital of Xi'an Jiaotong university. This study was approved by all researchers.

Consent for publication

All authors consent to submit the manuscript for publication.

Competing interests

The authors declare no competing interests.

Received: 22 January 2025 / Accepted: 6 April 2025

Published online: 19 April 2025

References

- Bray F, et al. Global cancer statistics 2022: GLOBOCAN estimates of incidence and mortality worldwide for 36 cancers in 185 countries. *CA Cancer J Clin.* 2024;74(3):229–63.
- Han B, et al. Cancer incidence and mortality in China, 2022. *J Natl Cancer Cent.* 2024;4(1):47–53.
- Zhang Y, et al. Global variations in lung cancer incidence by histological subtype in 2020: a population-based study. *Lancet Oncol.* 2023;24(11):1206–18.
- Abad E, Graifer D, Lyakhovich A. DNA damage response and resistance of cancer stem cells. *Cancer Lett.* 2020;474:106–17.
- Qie S, Sang N. Stanniocalcin 2 (*STC2*): a universal tumour biomarker and a potential therapeutic target. *J Exp Clin Cancer Res.* 2022;41(1):161.
- Qie S, et al. Stanniocalcin 2 governs cancer cell adaptation to nutrient insufficiency through alleviation of oxidative stress. *Cell Death Dis.* 2024;15(8):567.
- Lv H, et al. Analyzing the whole-transcriptome profiles of lncRNAs and predicting the competing endogenous RNA networks in cervical cancer cell lines with cisplatin resistance. *Cancer Cell Int.* 2021;21(1):532.
- Bu Q, et al. *STC2* is a potential biomarker of hepatocellular carcinoma with its expression being upregulated in *Nrf1*alpha-deficient cells, but downregulated in *Nrf2*-deficient cells. *Int J Biol Macromol.* 2023;253(Pt 8):127575.
- Li J, et al. Stanniocalcin-2 promotes cell EMT and Glycolysis via activating *ITGB2/FAK/SOX6* signaling pathway in nasopharyngeal carcinoma. *Cell Biol Toxicol.* 2022;38(2):259–72.
- Yun EJ, et al. Stanniocalcin 2 drives malignant transformation of human glioblastoma cells by targeting *SNAIL2* and matrix metalloproteinases. *Cell Death Discov.* 2022;8(1):308.
- He H, et al. Stanniocalcin 2 (*STC2*) expression promotes post-radiation survival, migration and invasion of nasopharyngeal carcinoma cells. *Cancer Manag Res.* 2019;11:6411–24.
- Jiang K, et al. *STC2* activates *PRMT5* to induce radioresistance through DNA damage repair and ferroptosis pathways in esophageal squamous cell carcinoma. *Redox Biol.* 2023;60:102626.
- Liu YN, et al. Acquired resistance to EGFR tyrosine kinase inhibitors is mediated by the reactivation of *STC2/JUN/AXL* signaling in lung cancer. *Int J Cancer.* 2019;145(6):1609–24.
- Pustovalova M et al. Transcriptome-Based traits of radioresistant sublines of Non-Small cell lung cancer cells. *Int J Mol Sci.* 2023. 24(3).
- Bischoff P, et al. Single-cell RNA sequencing reveals distinct tumor microenvironmental patterns in lung adenocarcinoma. *Oncogene.* 2021;40(50):6748–58.
- Li S, et al. Changing trends in the disease burden of esophageal cancer in China from 1990 to 2017 and its predicted level in 25 years. *Cancer Med.* 2021;10(5):1889–99.
- Alhaddad L et al. IR-Surviving NSCLC cells exhibit different patterns of molecular and cellular reactions relating to the multifraction irradiation regimen and p53-Family proteins expression. *Cancers (Basel).* 2021. 13(11).
- Li P, et al. The impact of Radioresistant-Related telomere genes in the prognosis and immune infiltration in lung adenocarcinoma. *Cancer Cell Int.* 2024;24(1):387.
- Chen Y, et al. Construction of a novel radioresistance-related signature for prediction of prognosis, immune microenvironment and anti-tumour drug sensitivity in non-small cell lung cancer. *Ann Med.* 2025;57(1):2447930.
- Wang M, et al. Radiation-induced *YAP/TEAD4* binding confers non-small cell lung cancer radioresistance via promoting *NRP1* transcription. *Cell Death Dis.* 2024;15(8):619.
- Li J, et al. Long non-coding RNA *CCAT1* acts as an oncogene to promote radiation resistance in lung adenocarcinoma: an epigenomics-based investigation. *Funct Integr Genomics.* 2024;24(2):52.
- Zhang Y, et al. Exosomal protein angiopoietin-like 4 mediated radioresistance of lung cancer by inhibiting ferroptosis under hypoxic microenvironment. *Br J Cancer.* 2022;127(10):1760–72.
- Chen Y, et al. Targeting *FBXO22* enhances radiosensitivity in non-small cell lung cancer by inhibiting the *FOXM1/Rad51* axis. *Cell Death Dis.* 2024;15(1):104.

24. Long HP, et al. PKMYT1 as a potential target to improve the radiosensitivity of lung adenocarcinoma. *Front Genet.* 2020;11:376.
25. Tian T, et al. HSD17B6 downregulation predicts poor prognosis and drives tumor progression via activating Akt signaling pathway in lung adenocarcinoma. *Cell Death Discov.* 2021;7(1):341.
26. Shen XJ, et al. Increased expression of stanniocalcin 2 is associated with tumor progression after radiotherapy in patients with cervical carcinoma. *Int J Clin Exp Pathol.* 2014;7(12):8770–6.

Publisher's note

Springer Nature remains neutral with regard to jurisdictional claims in published maps and institutional affiliations.